Defective DNA Polymerase α-Primase Leads to X-Linked Intellectual Disability Associated with Severe Growth Retardation, Microcephaly, and Hypogonadism

Hilde Van Esch,[1,2,*] Rita Colnaghi,[3] Kathleen Freson,[4] Petro Starokadomskyy,[5] Andreas Zankl,[6,7,8] Liesbeth Backx,[2] Iga Abramowicz,[3] Emily Outwin,[3] Luis Rohena,[9] Claire Faulkner,[10] Gary M. Leong,[11] Ruth A. Newbury-Ecob,[12] Rachel C. Challis,[13] Katrin Õunap,[14] Jacques Jaeken,[15] Eve Seuntjens,[16] Koen Devriendt,[1] Ezra Burstein,[5,17] Karen J. Low,[12] and Mark O'Driscoll[3,*]

Replicating the human genome efficiently and accurately is a daunting challenge involving the duplication of upward of three billion base pairs. At the core of the complex machinery that achieves this task are three members of the B family of DNA polymerases: DNA polymerases α, δ, and ε. Collectively these multimeric polymerases ensure DNA replication proceeds at optimal rates approaching 2×10^3 nucleotides/min with an error rate of less than one per million nucleotides polymerized. The majority of DNA replication of undamaged DNA is conducted by DNA polymerases δ and ε. The DNA polymerase α-primase complex performs limited synthesis to initiate the replication process, along with Okazaki-fragment synthesis on the discontinuous lagging strand. An increasing number of human disorders caused by defects in different components of the DNA-replication apparatus have been described to date. These are clinically diverse and involve a wide range of features, including variable combinations of growth delay, immunodeficiency, endocrine insufficiencies, lipodystrophy, and cancer predisposition. Here, by using various complementary approaches, including classical linkage analysis, targeted next-generation sequencing, and whole-exome sequencing, we describe distinct missense and splice-impacting mutations in *POLA1* in five unrelated families presenting with an X-linked syndrome involving intellectual disability, proportionate short stature, microcephaly, and hypogonadism. *POLA1* encodes the p180 catalytic subunit of DNA polymerase α-primase. A range of replicative impairments could be demonstrated in lymphoblastoid cell lines derived from affected individuals. Our findings describe the presentation of pathogenic mutations in a catalytic component of a B family DNA polymerase member, DNA polymerase α.

X-linked intellectual disability (XLID) is a heterogeneous disorder that can be classified as either non-syndromic, when cognitive impairment is the only feature, or as syndromic. In the latter, the cognitive impairment is associated with dysmorphic, metabolic, and/or neurological features. Until now, over 140 XLID-associated genes have been identified,[1] mainly through the implementation of comparative genome hybridization and next-generation sequencing technologies.[2,3] Many of these genes converge into a few common functional networks because ID proteins often participate in interconnected cellular and molecular processes, including neurogenesis, neuronal migration, and synapse formation and function.[4,5] Here, we report that hypomorphic defects in the replicative DNA polymerase α cause a human XLID syndrome. In five families, we identified mutations in *POLA1* (Xp22.1–p21.3, MIM: 312040), which encodes the p180 catalytic subunit of the heterotetrameric DNA polymerase α-primase (POLα). All affected individuals present with different degrees of intellectual disability and moderate to severe short stature, microcephaly, hypogonadism, and variable congenital malformations (Figure 1). Written informed consent was obtained from all parents on behalf of the affected individuals according to local ethical protocols and the principles of the Declaration of Helsinki. An overview of the clinical features of the affected individuals is presented in Table 1. More detailed clinical descriptions and pedigrees are provided in the Supplemental Note and Figure 1. The core clinical features consist of intellectual disability and developmental delay (ranging from mild to severe), pronounced proportionate short stature (ranging from −2 SD to −7.7 SD), and microcephaly (ranging from –3.1 SD to −7.8 SD), pointing toward a clear growth-deficiency syndrome of prenatal origin. Hypogonadism is also frequently evident. The index individual of family B also developed seizures and secondary

[1]Center for Human Genetics, University Hospitals Leuven, 3000 Leuven, Belgium; [2]Laboratory for the Genetics of Cognition, Department of Human Genetics, Katholieke Universiteit Leuven, 3000 Leuven, Belgium; [3]Genome Damage and Stability Centre, University of Sussex, BN1 9RQ Sussex, UK; [4]Department of Cardiovascular Sciences, Center for Molecular and Vascular Biology, Katholieke Universiteit Leuven, 3000 Leuven, Belgium; [5]Department of Internal Medicine, University of Texas Southwestern Medical Center, Dallas, TX 75390, USA; [6]Department of Clinical Genetics, the Children's Hospital at Westmead, Westmead, NSW 2145, Australia; [7]Children's Hospital Westmead Clinical School, Sydney Medical School, the University of Sydney, Westmead, NSW 2145, Australia; [8]Bone Biology Division and Kinghorn Centre for Clinical Genomics, Garvan Institute of Medical Research, Darlinghurst, NSW 2010, Australia; [9]Division of Genetics, Department of Pediatrics, San Antonio Military Medical Center, San Antonio, TX 78234, USA; [10]Bristol Genetics Laboratory, Southmead Hospital, BS10 5NB Bristol, UK; [11]Department of Paediatrics, Nepean Hospital, Nepean Clinical School, the University of Sydney, Kingswood, NSW 2747, Australia; [12]Clinical Genetics, St. Michael's Hospital, University Hospitals NHS Trust, BS2 8HW Bristol, UK; [13]MRC Human Genetics Unit, Institute of Genetics and Molecular Medicine, University of Edinburgh, EH4 2XU Edinburgh, UK; [14]Department of Clinical Genetics, United Laboratories, Tartu University Hospital and Institute of Clinical Medicine, University of Tartu, Tartu 50406, Estonia; [15]Center for Metabolic Diseases, University Hospitals Leuven, 3000 Leuven, Belgium; [16]Developmental Neurobiology, Department of Biology, Katholieke Universiteit Leuven, 3000 Leuven, Belgium; [17]Department of Molecular Biology, University of Texas Southwestern Medical Center, Dallas, TX 75390 Texas, USA
*Correspondence: hilde.vanesch@med.kuleuven.be (H.V.E.), m.o-driscoll@sussex.ac.uk (M.O.)
https://doi.org/10.1016/j.ajhg.2019.03.006.

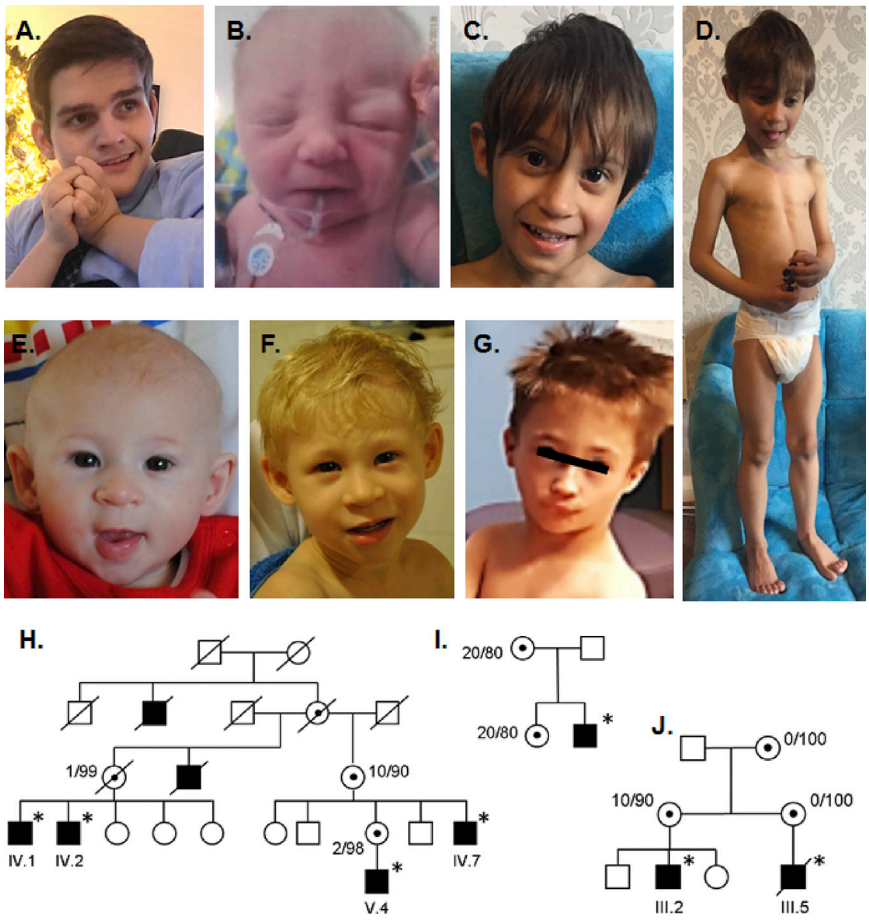

Figure 1. Clinical Pictures and Pedigrees
In clockwise order from top left: The index individual of family B at age 19 years (A); individual III-5 (family C) at newborn age (B); proband III-2 (family C) at age 5 years, demonstrating lack of subcutaneous fat, microcephaly, and proportionate short stature (C and D).
Lower panel: Pictures of the index individual of family D at age 6 months (E) and then at age 3 years (F); and a picture of the index individual of family E at the age of 4 years (G). All individuals displayed proportionate short stature and microcephaly, as well as a pronounced nasal bridge and a mild upslant of the palpebral fissures.
Below: Pedigrees of family A (H), family B (I), and family C (J). Carrier females showed skewing of X-inactivation (next to symbol). Asterisks indicate the affected individuals that were tested and carry the respective mutation.

neurological and orthopedic manifestations; these traits were not seen in the other individuals. In two affected individuals (in family C), a congenital heart malformation was present at birth. Although we cannot define a recognizable facial gestalt, mild upslant of the palpebral fissures is present in four affected individuals (Figures 1A–G).

Of the three mammalian replicative DNA polymerases (POLα, POLδ, and POLε), POLα-primase is the only polymerase that can initiate *de novo* DNA synthesis from licensed replication origins. It also mediates Okazaki-fragment synthesis during lagging-strand DNA replication.[6–8] POLα is also involved in other cellular processes such as DNA-damage-response signaling from stalled replication forks, telomere maintenance, and epigenetic regulation.[9–14] Interestingly, a recurrent, deep-intronic mutation in *POLA1* was recently found to cause X-linked reticulate pigmentary disorder (XLPDR; MIM: 301220), a primary immunodeficiency with autoinflammatory features, as well as skin hyperpigmentation and a prototypical facial gestalt.[15,16] This intronic mutation creates a novel exon 13a in the *POLA1* transcript, reducing the total amount of p180-POLα protein. XLPDR-affected individuals do not exhibit intellectual disability, altered body growth, or smaller head circumference, and this might indicate tissue-specific differences in abnormal splicing. Conversely, our affected individuals do not show any of the XLPDR-related symptoms, except proband E, who suffered from recurrent infections.

We identified *POLA1* mutations either by using classical linkage analysis and then Sanger sequencing of all 17 genes present in the 6 cM interval (LOD score 2.6) (family A),[17] by a custom-designed microcephaly/microcephalic dwarfism Sure Select capture panel consisting of 63 genes (family C), by single whole-exome sequencing (WES) (family B), or by trio WES (families D and E). In family A, a missense mutation in exon 3 of *POLA1* was identified, and this mutation, c.236T>G (p.Ile79Ser), segregates with the disease in all four affected individuals and obligate carrier mothers (Figure 1H). The sequence variant results in the replacement of an isoleucine, a non-polar amino acid, by a serine, a polar amino acid. This residue and its surrounding sequence are highly conserved, and p.IIe79Ser was predicted to be deleterious by various *in silico* methods (Figures S1 and S2). In family B, exome analysis identified a missense mutation, c.4142C>T, leading to a p.Pro1381Leu mutation. This mutation affects a conserved residue and is also present in the unaffected mother, maternal grandmother, and sister (Figures 1I, S1, and S2). In family C, a splice-site variant, c.507+1G>A, located in the donor splice site of intron 6 of *POLA1* was identified. The variant was identified in the affected proband and his affected maternal cousin (Figure 1J). The c.507+1G>A splice-site variant was predicted by five different splicing prediction programs to completely abolish the donor splice site. We performed RNA studies that showed that c.507+1G>A prevents normal splicing and leads to the production of two abnormally-spliced transcripts (Figure S1). The larger c.507+1G>A transcript results from the activation of a

Table 1. Overview of the Clinical Features of Affected Individuals

	Family A				Family B	Family C		Family D	Family E
	Individual V-4	Individual IV-7	Individual IV-1	Individual IV-2		Individual III-2	Individual III-5		
Gender	m	m	m	m	m	m	m	m	m
Country	Belgium				Belgium	UK		Australia	USA
Gene	*POLA1*				*POLA1*	*POLA1*		*POLA1*	*POLA1*
Chromosome change (Hg19), GenBank: NM_016937.3	c.236T>G				c.4142C>T	c.507+1G>A		c.445_507del	c.328G>A
Protein change	p.Ile79Ser				p.Pro1381Leu	p.Lys149_Glu169del, Thr170_Ser1462 delins15*		p.Lys149_Glu169del	p.Gly110Arg
Mutation type	missense				missense	splice site		in frame deletion exon 6	splice site
Birth Parameters									
Birth (weeks)	40 weeks	NA	NA	NA	39 weeks	38 weeks	38 weeks	38 weeks	29 weeks
Birth weight (g)	1,500 g	NA	NA	NA	2,700 g	1,786 g	1,729 g	1,688 g	840 g
Birth length (cm)	45 cm	NA	NA	NA	46.5 cm	NA	NA	44.5 cm	41 cm
Birth OFC (cm)	NA	NA	NA	NA	33 cm	30 cm	NA	28.5 cm	31.5 cm
Growth									
Age	6 years	28 years	46 years	44 years	16 years	5 years	14 months	6 years, 11 months	4 years, 5 months
Weight (kg)	10.5 kg (−7,9 SD)	NA	72 kg (+0.5 SD)	62 kg (−0.5 SD)	36.2 kg (−3.6 SD)	9.4 kg (−7 SD)	5.7 kg (−5 SD)	14.6 kg (−4.5 SD)	13.3kg (−1.9 SD)
Height (cm)	98 cm (−4 SD)	150 cm (−4.1 SD)	158 cm (−2.9 SD)	160 cm (−2.6 SD)	137 cm (−5 SD)	95.2 cm (−3.5 SD)	59 cm (−7.7 SD)	110.4 cm (−2.6 SD)	95.8cm (−2 SD)
OFC (cm)	42.9 cm (−5.7 SD)	47.7 cm (−4.9 SD)	51.2 cm (−2.9 SD)	49.7 cm (−3.7 SD)	49.4 cm (−3.7 SD)	41 cm (−7.8 SD)	38 cm (−6.6 SD)	43 cm (−5.8 SD)	46 cm (−3.1 SD)
Neurological									
Degree of DD/ID	mild (TIQ 71)	moderate (TIQ 57)	mild (TIQ 68)	moderate (TIQ 53)	severe	moderate	developmental delay	mild	mild (mainly speech delay)
Behavioral problems	ADHD	NP	NP	NP	hand stereotypies, autistic behavior	difficult behavior in association with frustration	NP	impulsive behavior, short attention span	shyness, weak eye contact, short attention
Hypotonia	childhood hypotonia	childhood hypotonia	NA	NA	childhood hypotonia	NP	yes	NP	yes

(*Continued on next page*)

Table 1. ***Continued***

	Family A				Family B	Family C		Family D	Family E
	Individual V-4	**Individual IV-7**	**Individual IV-1**	**Individual IV-2**		**Individual III-2**	**Individual III-5**		
Epilepsy	NP	NP	NP	NP	epilepsy from age 3 months, therapy resistant	NP	NP	NP	NP
Brain abnormalities and/or MRI	normal MRI imaging	normal MRI imaging	NA	NA	cerebellar atrophy	slight thickening of pituitary stalk	cerebral atrophy, postoperative left thalamic bleed	normal MRI imaging	normal MRI imaging
Other	–	–	–	–	spasticity	–	vocal cord palsy	–	–
Facial Features									
Dysmorphic features	retrognathia	NP	NP	NP	large mouth, downturned corners of the mouth	short palpebral fissures; upslanting, prominent ears; brachymesophalangy	retrognathia, flat nasal bridge, small nose	upslanting palpebral fissures, long face	small ears, shallow orbits, upslanting palpebral fissures, fifth finger clinodactyly
Gastro-Intestinal									
	NP	NP	NP	NP	gastrostomy	esophageal atresia with tracheosophageal fistula (repaired postnatal day 3)	NP	NP	tube feeding
Heart									
	normal	NA	NA	NA	normal	small ASD	pulmonary artery stenosis, VSD, pulmonary atresia	normal	normal
Urogenital and Endocrine									
Hypogonadotropic hypogonadism	NA	yes	yes	yes	yes, small testes (10 ml)	NA	yes	NA	left testicular atrophy, small right testicle
Senses									
Vision	normal	normal	normal	normal	normal	normal	normal	normal	intermittent esotropia, astigmatism
Other	–	–	–	NIDDM	secondary scoliosis	sacral dimples	sacral dimples, bifid uvula	–	recurrent infections

Abbreviations are as follows: NA = not assessed; NP = not present; OFC = occipital frontal circumference; ASD = atrial septum defect; NIDDM = non-insulin-dependent diabetes; ADHD = attention deficit hyperactivity disorder; VSD = ventral septal defect; and TIQ = total intelligence quotient.

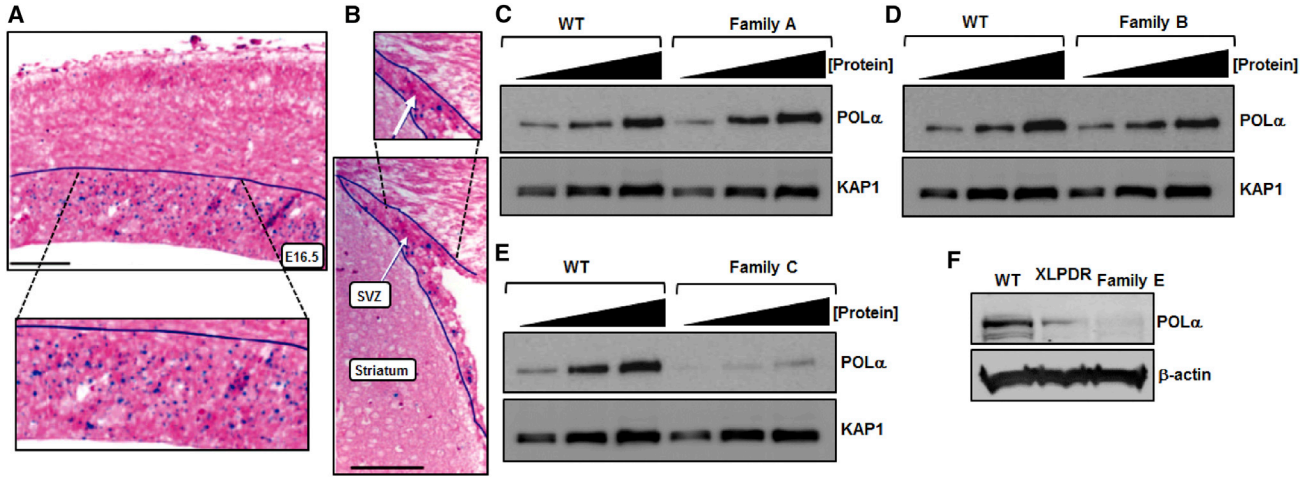

Figure 2. *Pola1* Is Expressed in Proliferating Progenitors During Embryonic and Postnatal Neurogenesis in the Mouse Brain, and *POLA1*-Mutated Cells Exhibit Variable POLα Expression

(A) The *Pola1* transcript (dark blue signal) is found in the proliferative zone of the embryonic neocortex. The scale bar represents 200 μm. The dashed lines indicate an expanded area of the image.

(B) Three weeks after birth, *Pola1* (dark blue signal) is expressed in the subventricular zone (SVZ), where postnatal neurogenesis occurs. The scale bar represents 200 μm. The dashed lines indicate an expanded area of the image.

(C) Increasing amounts of whole-cell extract (WCE) from LCLs derived from a clinically unaffected, unrelated, normal wild-type (WT) male individual and a *POLA1*-mutant-affected individual from family A were assessed for POLα expression levels. No difference in expression was observed.

(D) Increasing amounts of WCE from LCLs derived from the WT and a *POLA1*-mutant-affected individual from family B were assessed for POLα expression levels. POLα expression was comparable.

(E) Increasing amounts of WCE from LCLs derived from the WT and a *POLA1*-mutant-affected individual from family C were assessed for POLα expression levels. Here, POLα was markedly reduced in affected cells compared to in WT LCLs.

(F) POLα levels were assessed via WCE derived from dermal fibroblasts from the WT, an XLPDR-affected individual, and the *POLA1*-mutant-affected individual from family E. POLα was reduced in both instances of *POLA1* mutation.

cryptic splice donor site within intron 6, leading to an insertion of the first 60 nucleotides of intron 6. This is predicted to cause an insertion of 15 amino acids and the introduction of a premature termination codon, p.Thr170_Ser1462delins15*, truncating the potential p180-POLα product upstream of the domains responsible for DNA binding and catalytic activity. The smaller c.507+1G>A transcript results from exon 6 skipping and leads to an in-frame deletion, i.e., p.Lys149_Glu169del, that is predicted to produce a protein product lacking 21 amino acids (Figure S1). In family D, a hemizygous deletion of exon 6 was identified via exome sequencing, and this deletion led to an in-frame deletion producing a protein lacking 21 amino acids, as seen for the smaller transcript in family C. This deletion arose *de novo* in the index individual (Figure S1). Exome sequencing in family E identified a *de novo* variant, c.328G>A, affecting the last nucleotide of exon 4 and leading to a p.Gly110Arg mutation. Bioinformatic analysis predicts a high probability of intron 4 missplicing upon c.328G>A replacement, and subsequent qRT-PCR analysis displayed a dramatic reduction of *POLA1* mRNA in affected cells compared to cells derived from unaffected males; the reduction was even more profound than that observed in XLPDR-derived fibroblasts[15] (Figure S1). None of the above identified variants are present in the dbSNP, 1000 Genomes, ExAC, or gnomAD databases, and we have submitted them to ClinVar (see Accession Numbers). All missense mutations affect conserved amino acids and are predicted to be deleterious by various *in silico* methods (Figure S2). In addition, in the three familial cases (families A–C), all obligate female carriers show significant to complete skewing of X inactivation (Figures 1H–J).

DNA polymerases are highly expressed during development, when rapid DNA replication and cell division is required.[18,19] To further investigate POLα/*POLA1* in mammalian brain development, we assessed *Pola1* expression by *in situ* hybridization in the embryonic and adult mouse brain. In the mouse forebrain, *Pola1* is expressed in those zones containing proliferating cells in the developing embryonic neocortex (Figure 2A), as well as in the lateral and medial ganglionic eminences (not shown). After birth, the gene is transcribed in cells that remain proliferating in the ventricular and subventricular zone of the striatum (Figure 2B). These data suggest that *Pola1* has a role in neurogenesis throughout life. Additionally, *pola1* expression by *in situ* hybridization in developing zebrafish embryos shows early and intense staining in the developing brain,[20,21] whereas Polα activity appears highest in isolated neurons from developing rat-brain cerebral cortex when the mitotic activity is at its peak.[22] Conversely, an insertional mutation in zebrafish *pola1* (*pola1*^{hi1146Tg}) led to central nervous system (CNS) necrosis, a small head and eyes, an inflated hindbrain ventricle, a thin and often curved body, and a rounder yolk with no extension at day 2.[23] At days 3–5, the necrosis spread throughout the body, resulting in overt body wasting and a small head and eyes.[23]

We examined POLα protein levels in proband-derived cell lines from families A, B, C, and E (Figures 2C–F). Cell lines from the family D proband were unavailable. By using whole-cell extracts (WCEs) from lymphoblastoid cell lines (LCLs) derived from affected individuals from families A and B, we found POLα protein levels comparable to those of wild-type (WT) LCLs (Figures 2C and 2D). In contrast, WCEs derived from the family C proband's LCLs or from dermal, primary fibroblasts from the family E proband both showed marked reduction in POLα levels (Figures 2E and 2F). These findings are consistent with the RT-PCR analysis from each of these two families (Figure S1). We next assessed POLα enrichment on chromatin by using LCLs derived from affected individuals. Although chromatin extracts from families A and B tended toward slightly reduced POLα levels compared to those of WT LCLs, the reduction did not reach statistical significance (Figures S3A and S3B). In contrast, chromatin extracts from family C's LCLs showed an approximately 60% reduction in POLα levels compared to those of WT LCLs (Figure S3C). Furthermore, chromatin recruitment of the additional POLα-primase subunit proteins p68-POLA2 and p48-PRIM1 appeared unaffected in proband LCL extracts from families A, B, and C, suggesting the stoichiometry of the POLα-primase component subunits is largely preserved (Figure S3D).

Reduced cellular proliferation represents a logical pathomechanism underlying growth retardation and microcephaly in human disorders such as Seckel syndrome (MIM: 210600), which presents with prototypical microcephalic primordial dwarfism, or Meier-Gorlin syndrome (MIM: 224690), in which the dwarfism is caused by mutations in multiple components of the DNA replication-licensing machinery.[24–26] The *C.elegans div-1* (division delayed) allele encoding the B subunit of DNA polymerase α-primase delays cell division and lethally disrupts cell polarity in embryos,[27] whereas *POL1* mutants of *S. cerevisiae* and a *Pola1* mutant (p.Ser1180Phe) of the mouse mammary carcinoma line FM3A are each associated with temperature-sensitive growth delay.[11,28] Nonetheless, we did not observe a marked delay in proliferation of proband LCLs from families A, B, and C compared to in the WT (Figure S4). Therefore, we carefully assessed different aspects of DNA-replication capacity in family C's LCLs specifically, as these showed a pronounced reduction in POLα-primase expression and chromatin localization (Figures 2E and S3C). POLα is characterized by limited processivity, and it also lacks 3′ exonucleolytic proofreading capacity. Therefore, in contrast to POLδ and POLε, POLα is unsuited to efficiently and accurately duplicate long DNA templates.[29,30] By using DNA-fiber-combing analysis of ongoing, unperturbed DNA replication in LCLs obtained from the proband of family C and his unaffected father, we observed similar rates of replication-fork progression (Figure 3A). This was perhaps not entirely unanticipated because POLα-primase doesn't replicate the bulk of the genomic DNA, and *POLA1* encodes a core product of a fundamentally essential cellular process, hence any viable defects in this gene would have to be hypomorphic. POLα is essential for viability;[23,27,31] indeed, *POLA1* has a negative residual-variation intolerance score of −0.795, indicating it is under substantial purifying selection.[15,32] This is further illustrated by the absence of microdeletions involving *POLA1* in males, both in the control and diseases copy number variation (CNV) databases, as well as by the identification of a female with X-autosome translocation-disrupting *POLA1*. In this female, in contrast to what normally happens, the wild-type X chromosome remained active in all her cells, probably as a result of selection against cells that contained the non-functional *POLA1*.[33] DNA-fiber-combing analysis did reveal a reduction in new initiation events in the family C proband's LCLs of 5.9% (n = 170 fibers), compared to 9.6% (n = 178 fibers) observed in the paternal LCLs, a difference indicative of impaired "productive" replication initiation.[34,35] Consistent with this, we also observed increased inter-origin distance (IOD) in the family C proband's LCLs compared to those of the father (Figure 3B). This would also be consistent with possible impairments in dormant origin firing.[34,35] Furthermore, we found an increase in asymmetric forks and an accumulation of longer replication tracts in the family C proband's LCLs compared to those of the father (Figures 3C and 3D). Collectively, analyses of multiple replication-fork parameters in these *POLA1*-deficient LCLs demonstrated several phenotypes consistent with spontaneously diminished productive-replication initiation under unperturbed exponential growth conditions. These replication phenotypes are reminiscent of those recently reported for Polε impairment.[36]

We next reasoned that additional impairments of DNA replication in *POLA1* LCLs could be context dependent, and DNA replication under conditions of replication stress may represent that physiological context.[37] Disrupting the temporally coordinated balance between stem-cell proliferation and differentiation programs profoundly impacts upon brain and body growth.[38,39] Rapidly proliferating murine embryonic stem cells exhibit constitutive replication stress and are highly dependent on replication-coupled pathways to preserve genome integrity and execute DNA replication efficiently and effectively.[40] Therefore, we reasoned that DNA replication in *POLA1*-mutated cells may be hypersensitive to replication-stress conditions, particularly if dormant origin capacity was restricted due to a genetic defect of this nature.[34,35] We examined DNA fibers under conditions of replication stress by limiting deoxyribonucleotide availability via treatment with the ribonucleotide reductase inhibitor hydroxyurea (HU), and we observed an approximately 2-fold increase in stalled replication forks in combed fibers from the family C proband's LCLs compared to paternal LCLs (Figure 4A). We next assessed DNA replication via pulse-labeled EdU incorporation within LCL populations in a kinetic fashion after HU treatment (Figures 4B–D). Figure 4B shows representative EdU flow-cytometry profiles from family C paternal

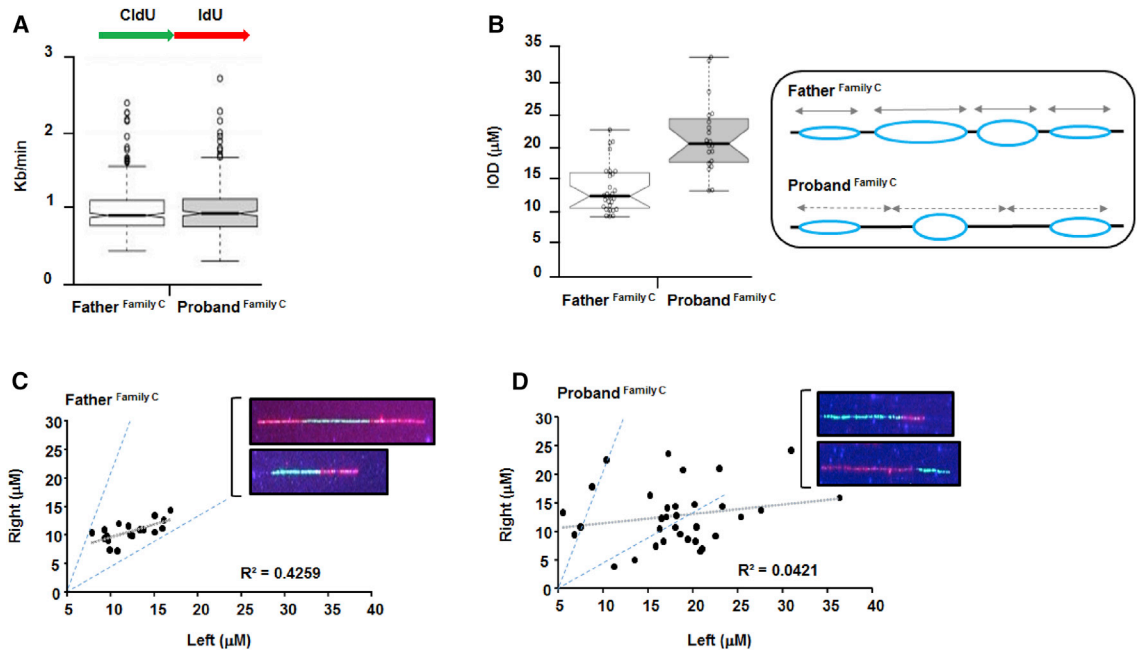

Figure 3. ***POLA1*-Mutant LCLs Spontaneously Exhibit a Range of DNA-Replication Defects During Unperturbed, Exponential Growth**
(A) Dual CldU (5-Chloro-2′-deoxyuridine)- and IdU (5-Iodo-2′-deoxyuridine)-labeled (for 20 min each, as indicated) DNA-fiber-combing analyses of unperturbed, exponentially growing LCLs from the unaffected father and family C proband (individual III-2) demonstrated similar replication-fork speeds between the fathers' LCLs (mean: 0.95kb/min, median: 0.89, from n = 615 fibers) and the family C proband's (mean: 1.01kb/min, median: 1.01kb/min, from n = 926 fibers). CldU fibers are shown in green and IdU fibers are shown in red.
(B) Origins from the family C proband's (individual III-2) LCLs exhibited significantly elevated inter-origin distance (IOD) compared to that in those of the father during unperturbed, asynchronous growth conditions. The father's IOD median was 12.62 μM (n = 28), compared to the family C proband's IOD median of 20.75 μM (n = 20) ($p < 0.05$; Student's t test). The schematic idealizes the most likely contrasting situation with regard to the bidirectional movement of fired origins (blue) in the father's LCLs compared to that in those of the proband. In the proband, fewer new initiation events are seen (i.e., fewer new origins and reduced dormant origin-firing capacity), and those that have fired are thus compelled to traverse greater distances.
(C) In the *XY* scatterplot, the data show the length of fibers on the right- and left-hand-sides of fired origins and/or ongoing forks, visualized after the father's LCLs were subjected to DNA fiber combing. Normally, functional replicating forks exhibit left-right symmetry reflective of coordinated bidirectional movement. The dotted gray line indicates linear regression ($R^2 = 0.4259$ from n = 18) showing a strong clustering, which is consistent with symmetrical movement, of the forks. The dotted blue lines are guide lines drawn to encapsulate the lengths of all of the forks assessed. Representative symmetrical fibers from the paternal LCLs are shown inset.
(D) This *XY* scatterplot shows the length of fibers on the right- and left-hand-sides of fired origins and/or ongoing forks derived from the family C proband's LCLs. The wide dispersal of the data points with regard to the blue guide lines (copied from the paternal XY scatterplot shown in [C]) indicates marked asymmetric movement of active replication forks. The dotted gray line denotes linear regression ($R^2 = 0.0421$ from n = 33). Note also the preponderance of longer fork lengths (i.e., >15 μM) observed in these fibers compared to the lengths of those of the father's fibers (shown in [C]). Representative fibers that are derived from the family C proband's LCLs and that demonstrate asymmetry are shown inset.

and proband LCLs, either untreated (Unt) or at different times after HU treatment. The family C proband's LCLs incorporated significantly less EdU upon HU-treatment compared to control LCLs (Figures 4B and 4C). This is a *POLA1*-dependent cellular phenotype, as demonstrated by siRNA of *POLA1* in U2OS cells (Figure S5). Similarly, after treatment with HU, proband LCLs from family A and family B exhibited significantly reduced EdU incorporation, which is indicative of impaired DNA replication (Figure 4D). Collectively, these results show that LCLs from affected individuals with distinct *POLA1* mutations exhibit reduced DNA replication under conditions of replication stress. A similar cellular response has been demonstrated for *ORC1*-mutated (MIM: 224690) and *MCM5*-mutated Meier-Gorlin syndrome (MIM: 617564) LCLs.[41,42] Indeed, pathogenic mutations in *MCM4* (MIM: 609981) and in the *GINS1* (MIM: 617827) component of the heterotetrametic Go-Ichi-Ni-San (GINS) complex, both encoding key components of the DNA replication apparatus, are each associated with cellular-proliferation impairments, growth delay, and natural killer (NK) cell deficiency.[43–45]

In summary, we describe nine affected individuals, from five families, who present with a syndrome involving a spectrum of developmental delay/intellectual disability, growth failure, microcephaly, hypogonadism, and additional, isolated abnormalities; this syndrome is associated with five different mutations in *POLA1*, which encodes the catalytic subunit of the DNA polymerase α-primase. The growth impairments were evident prenatally, suggesting an early origin *in utero*. LCLs from the proband of one affected family spontaneously displayed altered replication-fork parameters, including reduced new-initiation events, increased IOD and fork asymmetry, and elongated replication tracts. All the *POLA1*-mutant LCLs we

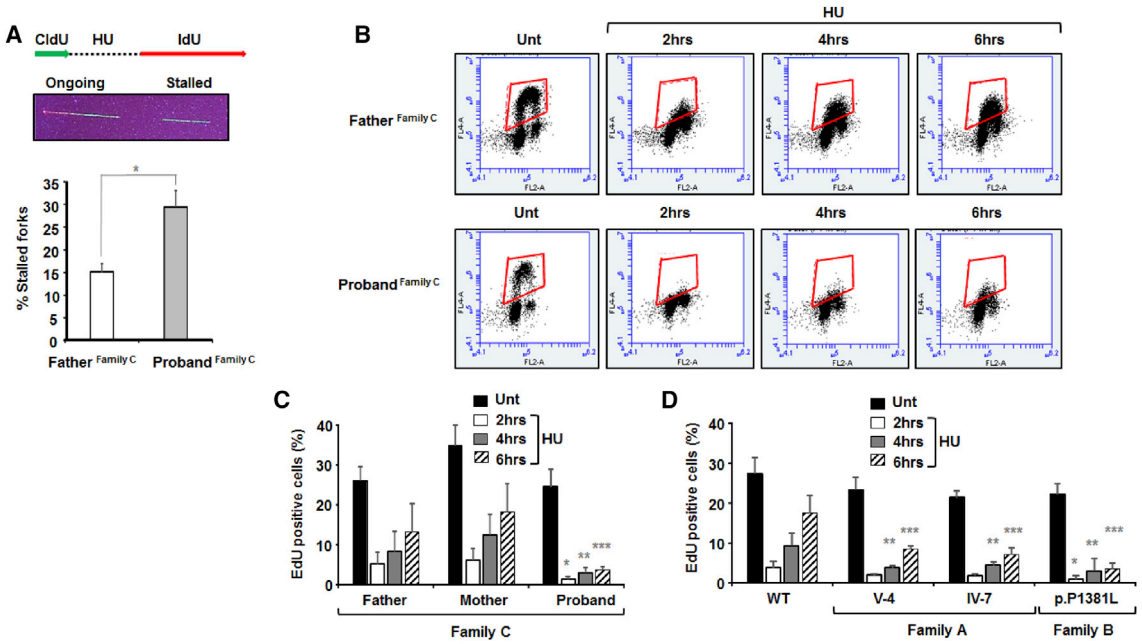

Figure 4. *POLA1*-Mutant Proband LCLs Exhibit DNA-Replication Deficits After Experiencing Replication Stress

(A) The level of replication-fork stalling was investigated via a dual CldU- and IdU-labeling approach that incorporated a hydroxyurea (HU) treatment. LCLs were first labeled with CldU (for 20 min) and then treated with HU (2 mM, for 120 mins) before a second labeling with IdU (for 60 mins) to monitor fork recovery, as indicated. The middle panel shows a representative image of a labeled fiber demonstrating ongoing replication and a stalled replication fork. Under these conditions, an approximately 2-fold increase in the levels of stalled replication forks was observed in LCLs from the family C proband, relative to the levels in the paternal LCLs (*$p < 0.05$, Student's t test; error bars = standard deviation).

(B) The impact of mildly stressing conditions (125 μM HU) upon DNA replication was assessed in LCLs from family C via EdU-pulse incorporation (for 30 min) and flow cytometry. Representative flow cytometry panels are shown; the area boxed in red denotes EdU-positive cells. LCLs derived from the unaffected father and the proband were either untreated (Unt) or treated with HU, and EdU incorporation was measured at the times indicated post-treatment. Consistent with the DNA-fiber fork-rate analysis shown in Figure 3A, EdU incorporation in untreated LCLs was grossly comparable between the father and the proband. This was in contrast to the HU-treated LCLs, where the proband showed markedly fewer EdU-positive cells at each time point compared to the father.

(C) The bar chart shows EdU incorporation in untreated (Unt) and HU-treated LCLs from the father, mother, and proband of family C from 4× independent experiments (asterisks indicate $p < 0.05$ [Student's t test], compared to the equivalent parental time points; error bars = standard deviation). The proband LCLs demonstrate significantly reduced EdU incorporation at each time point after HU treatment, compared to the parental LCLs under these conditions.

(D) The bar chart shows EdU incorporation in untreated (Unt) and HU-treated LCLs from a clinically normal, unrelated, wild-type (WT) male individual and affected individuals from family A and family B from 4× independent experiments (asterisks indicate $p < 0.05$ [Student's t test], compared to the equivalent WT time point; error bars = standard deviation). LCLs from all of the probands demonstrate significantly reduced EdU incorporation compared to WT LCLs after HU treatment. This was most evident at 4 and 6 hr post-HU treatment.

examined were additionally found to exhibit impaired DNA-replication capacity under conditions of replication stress. These data strongly suggest that cellular DNA-replication deficits during development may underlie many of the clinical features observed in these families.

Interestingly, a recurrent intronic variant in *POLA1* has been shown to underlie XLPDR, a primary immunodeficiency associated with type I-interferon-derived autoinflammatory features.[15] The elevated type I-interferon-signaling response underlying XLPDR has been shown to derive from a reduction in POLα-dependent synthesis of cytosolic RNA:DNA hybrid species.[15] Importantly, XLPDR cells with this specific intronic *POLA1* variant do not exhibit a proliferative impairment and, except for the recurrent infections observed in proband E, we observed no other phenotypic overlap with XLPDR.[15]

The remarkable fidelity of human DNA replication is a consequence of the combined and coordinated action of highly processive DNA polymerases, their intrinsic exonucleolytic proofreading activity, and post-replicative DNA mismatch repair (MMR). Although POLα-primase initiates DNA replication and Okazaki-fragment synthesis, it is not highly processive and does not possess an intrinsic proofreading activity. Processivity and proofreading are carried out by POLδ and POLε.[29] Germline mutations in components of the MMR pathway result in dramatically elevated spontaneous mutation frequencies and are associated with hereditary, non-polyposis colorectal carcinoma (HNPCC) or Lynch syndrome (MIM: 120435).[46,47] Germline mutations within the exonucleolytic, domain-encoding regions of *POLD1* (MIM: 174761) and *POLE* (MIM: 174762), each encoding the catalytic subunit of the replicative polymerases POLδ and POLε, respectively, have been identified as causing ultra-mutated colorectal ("polymerase proofreading-associated polyposis") and endometrial cancers (MIM: 612591 and 615083).[48–51]

Fascinatingly, differing mutations in *POLE* underlie a clinical spectrum that includes FILS syndrome (facial dysmorphism, immunodeficiency, livedo reticularis, and short stature; MIM: 615083)[52] and IMAGe syndrome (intrauterine growth restriction, metaphyseal dysplasia, adrenal hypoplasia, and congenital and genitourinary anomalies in males; MIM: 614732), and both diseases are associated with variable immunodeficiency.[36,53] Additionally, a *POLE2* (MIM: 602670) mutation has been identified in an individual with combined immunodeficiency, facial dysmorphism, and autoimmunity associated with compromised lymphocyte proliferation.[54] Germline mutations in *POLD1* have been described to underlie a range of congenital disorders, including MDP syndrome (mandibular hypoplasia, deafness, and progeroid; MIM: 615381), lipodystrophy, and atypical Werner's syndrome with short stature (MIM: 277700).[55–60] Therefore, it appears that germline mutations in the core DNA-replication polymerases can present as a wide range of phenotypes and variably incorporate cancer predisposition, developmental and/or progeroid syndromes with or without growth failure, endocrine insufficiency, and variable immunodeficiency. Our findings make an important additional contribution to this expanding knowledge base: namely, that hitherto-undescribed hypomorphic *POLA1* mutations affecting the catalytic subunit of DNA POLα-primase are associated with multifaceted cellular DNA-replicative deficits, and they underlie an X-linked syndrome of intellectual disability, microcephaly, growth failure, and hypogonadism.

Accession Numbers

ClinVar accession numbers for the variants reported in this paper were not available from ClinVar as of the date this article was finalized for press; please contact the corresponding authors for the numbers.

Supplemental Data

Supplemental Data can be found online at https://doi.org/10.1016/j.ajhg.2019.03.006.

Acknowledgments

The authors thank the families for their cooperation and acknowledge Andrew Jackson for helpful comments and assistance, Mark Greenslade for his work at Bristol Genetics Laboratory with family C, and Claudia Kerzendorfer for her contributions to the functional characterization of cells from family A. Thanks also to Adam Lopez, Luis Situentes-Dominguez, and Ann Ray. H.V.E. and K.D. are clinical investigators of the Fund for Scientific Research Flanders (FWO-Vlaanderen), Belgium. M.O'D. acknowledges program funding from Cancer Research UK (United Kingdom). Work with family E was supported by funds to E.B from the Pollock Family Center for Research in Inflammatory Bowel Disease.

Declaration of Interests

The authors declare no competing interests.

Received: December 8, 2018
Accepted: March 4, 2019
Published: April 18, 2019

Web Resources

1000 Genomes, http://www.internationalgenome.org/
Align-GVGD, http://agvgd.hci.utah.edu/
ClinVar, https://www.ncbi.nlm.nih.gov/clinvar/
dbSNP, https://www.ncbi.nlm.nih.gov/snp
ExAC, http://exac.broadinstitute.org/
Genic Intolerance, http://genic-intolerance.org/index.jsp
gnomAD, https://gnomad.broadinstitute.org/
MutationTaster, http://mutationtaster.org/
Online Mendelian Inheritance in Man, http://www.omim.org
Provean (Protein Variation Effect Analyzer), http://provean.jcvi.org/index.php
PolyPhen, http://genetics.bwh.harvard.edu/pph/

References

1. Neri, G., Schwartz, C.E., Lubs, H.A., and Stevenson, R.E. (2018). X-linked intellectual disability update 2017. Am. J. Med. Genet. A. *176*, 1375–1388.
2. Aerts, S., Lambrechts, D., Maity, S., Van Loo, P., Coessens, B., De Smet, F., Tranchevent, L.-C., De Moor, B., Marynen, P., Hassan, B., et al. (2006). Gene prioritization through genomic data fusion. Nat. Biotechnol. *24*, 537–544.
3. Tarpey, P.S., Smith, R., Pleasance, E., Whibley, A., Edkins, S., Hardy, C., O'Meara, S., Latimer, C., Dicks, E., Menzies, A., et al. (2009). A systematic, large-scale resequencing screen of X-chromosome coding exons in mental retardation. Nat. Genet. *41*, 535–543.
4. Chelly, J., Khelfaoui, M., Francis, F., Chérif, B., and Bienvenu, T. (2006). Genetics and pathophysiology of mental retardation. Eur. J. Hum. Genet. *14*, 701–713.
5. Gécz, J., Shoubridge, C., and Corbett, M. (2009). The genetic landscape of intellectual disability arising from chromosome X. Trends Genet. *25*, 308–316.
6. Burgers, P.M.J., and Kunkel, T.A. (2017). Eukaryotic DNA replication fork. Annu. Rev. Biochem. *86*, 417–438.
7. Burgers, P.M.J. (2009). Polymerase dynamics at the eukaryotic DNA replication fork. J. Biol. Chem. *284*, 4041–4045.
8. Stodola, J.L., and Burgers, P.M. (2017). Mechanism of Lagging-Strand DNA Replication in Eukaryotes. In DNA Replication: From Old Principles to New Discoveries, H. Masai and M. Foiani, eds. (Singapore: Springer Singapore), pp. 117–133.
9. Yan, S., and Michael, W.M. (2009). TopBP1 and DNA polymerase-α directly recruit the 9-1-1 complex to stalled DNA replication forks. J. Cell Biol. *184*, 793–804.
10. Michael, W.M., Ott, R., Fanning, E., and Newport, J. (2000). Activation of the DNA replication checkpoint through RNA synthesis by primase. Science *289*, 2133–2137.
11. Nakamura, M., Nabetani, A., Mizuno, T., Hanaoka, F., and Ishikawa, F. (2005). Alterations of DNA and chromatin structures at telomeres and genetic instability in mouse cells defective in DNA polymerase α. Mol. Cell. Biol. *25*, 11073–11088.
12. Nakayama Ji, Allshire, R.C., Klar, A.J.S., and Grewal, S.I.S. (2001). A role for DNA polymerase alpha in epigenetic control of transcriptional silencing in fission yeast. EMBO J. *20*, 2857–2866.

13. Wallace, J.A., and Orr-Weaver, T.L. (2005). Replication of heterochromatin: Insights into mechanisms of epigenetic inheritance. Chromosoma *114*, 389–402.
14. Gilbert, D.M. (2002). Replication timing and transcriptional control: Beyond cause and effect. Curr. Opin. Cell Biol. *14*, 377–383.
15. Starokadomskyy, P., Gemelli, T., Rios, J.J., Xing, C., Wang, R.C., Li, H., Pokatayev, V., Dozmorov, I., Khan, S., Miyata, N., et al. (2016). DNA polymerase-α regulates the activation of type I interferons through cytosolic RNA:DNA synthesis. Nat. Immunol. *17*, 495–504.
16. Starokadomskyy, P., Sifuentes-Dominguez, L., Gemelli, T., Zinn, A.R., Dossi, M.T., Mellado, C., Bertrand, P., Borzutzky, A., and Burstein, E. (2017). Evolution of the skin manifestations of X-linked pigmentary reticulate disorder. Br. J. Dermatol. *177*, e200–e201.
17. Van Esch, H., Zanni, G., Holvoet, M., Borghgraef, M., Chelly, J., Fryns, J.-P., and Devriendt, K. (2005). X-linked mental retardation, short stature, microcephaly and hypogonadism maps to Xp22.1-p21.3 in a Belgian family. Eur. J. Med. Genet. *48*, 145–152.
18. Srivastava, V.K., and Busbee, D.L. (2003). Replicative enzymes, DNA polymerase alpha (pol alpha), and in vitro ageing. Exp. Gerontol. *38*, 1285–1297.
19. Loeb, L.A., and Monnat, R.J., Jr. (2008). DNA polymerases and human disease. Nat. Rev. Genet. *9*, 594–604.
20. Thisse, B., and Thisse, C. (2004). Fast release clones: A high throughput expression analysis. ZFIN Direct Data Submission. http://zfin.org/ZDB-PUB-040907-1.
21. Thisse, B., Pflumio, S., Fürthauer, M., Loppin, B., Heyer, V., Degrave, A., Woehl, R., Lux, A., Steffan, T., Charbonnier, X.Q., and Thisse, C. (2001). Expression of the zebrafish genome during embryogenesis (NIH R01 RR15402). ZFIN Direct Data Submission. http://zfin.org/ZDB-PUB-010810-1.
22. Raji, N.S., Krishna, T.H., and Rao, K.S. (2002). DNA-polymerase α, β, δ and ε activities in isolated neuronal and astroglial cell fractions from developing and aging rat cerebral cortex. Int. J. Dev. Neurosci. *20*, 491–496.
23. Amsterdam, A., Nissen, R.M., Sun, Z., Swindell, E.C., Farrington, S., and Hopkins, N. (2004). Identification of 315 genes essential for early zebrafish development. Proc. Natl. Acad. Sci. USA *101*, 12792–12797.
24. Alcantara, D., and O'Driscoll, M. (2014). Congenital microcephaly. Am. J. Med. Genet. C. Semin. Med. Genet. *166C*, 124–139.
25. O'Driscoll, M. (2017). The pathological consequences of impaired genome integrity in humans; disorders of the DNA replication machinery. J. Pathol. *241*, 192–207.
26. Klingseisen, A., and Jackson, A.P. (2011). Mechanisms and pathways of growth failure in primordial dwarfism. Genes Dev. *25*, 2011–2024.
27. Encalada, S.E., Martin, P.R., Phillips, J.B., Lyczak, R., Hamill, D.R., Swan, K.A., and Bowerman, B. (2000). DNA replication defects delay cell division and disrupt cell polarity in early Caenorhabditis elegans embryos. Dev. Biol. *228*, 225–238.
28. Gutiérrez, P.J.A., and Wang, T.S.-F. (2003). Genomic instability induced by mutations in Saccharomyces cerevisiae POL1. Genetics *165*, 65–81.
29. Kunkel, T.A., and Burgers, P.M. (2008). Dividing the workload at a eukaryotic replication fork. Trends Cell Biol. *18*, 521–527.
30. Pavlov, Y.I., Frahm, C., Nick McElhinny, S.A., Niimi, A., Suzuki, M., and Kunkel, T.A. (2006). Evidence that errors made by DNA polymerase α are corrected by DNA polymerase δ. Curr. Biol. *16*, 202–207.
31. Eki, T., Enomoto, T., Murakami, Y., Hanaoka, F., and Yamada, M. (1987). Characterization of chromosome aberrations induced by incubation at a restrictive temperature in the mouse temperature-sensitive mutant tsFT20 strain containing heat-labile DNA polymerase α. Cancer Res. *47*, 5162–5170.
32. Petrovski, S., Wang, Q., Heinzen, E.L., Allen, A.S., and Goldstein, D.B. (2013). Genic intolerance to functional variation and the interpretation of personal genomes. PLoS Genet. *9*, e1003709.
33. Podolska, A., Kobelt, A., Fuchs, S., Hackmann, K., Rump, A., Schröck, E., Kutsche, K., and Di Donato, N. (2017). Functional monosomy of 6q27-qter and functional disomy of Xpter-p22.11 due to X;6 translocation with an atypical X-inactivation pattern. Am. J. Med. Genet. A. *173*, 1334–1341.
34. McIntosh, D., and Blow, J.J. (2012). Dormant origins, the licensing checkpoint, and the response to replicative stresses. Cold Spring Harb. Perspect. Biol. *4*, a012955.
35. Alver, R.C., Chadha, G.S., and Blow, J.J. (2014). The contribution of dormant origins to genome stability: From cell biology to human genetics. DNA Repair (Amst.) *19*, 182–189.
36. Bellelli, R., Borel, V., Logan, C., Svendsen, J., Cox, D.E., Nye, E., Metcalfe, K., O'Connell, S.M., Stamp, G., Flynn, H.R., et al. (2018). Polε instability drives replication stress, abnormal development, and tumorigenesis. Mol. Cell *70*, 707–721.e7.
37. Kotsantis, P., Petermann, E., and Boulton, S.J. (2018). Mechanisms of oncogene-induced replication stress: Jigsaw falling into place. Cancer Discov. *8*, 537–555.
38. Arai, Y., Pulvers, J.N., Haffner, C., Schilling, B., Nüsslein, I., Calegari, F., and Huttner, W.B. (2011). Neural stem and progenitor cells shorten S-phase on commitment to neuron production. Nat. Commun. *2*, 154.
39. Dehay, C., and Kennedy, H. (2007). Cell-cycle control and cortical development. Nat. Rev. Neurosci. *8*, 438–450.
40. Ahuja, A.K., Jodkowska, K., Teloni, F., Bizard, A.H., Zellweger, R., Herrador, R., Ortega, S., Hickson, I.D., Altmeyer, M., Mendez, J., and Lopes, M. (2016). A short G1 phase imposes constitutive replication stress and fork remodelling in mouse embryonic stem cells. Nat. Commun. *7*, 10660.
41. Kerzendorfer, C., Colnaghi, R., Abramowicz, I., Carpenter, G., and O'Driscoll, M. (2013). Meier-Gorlin syndrome and Wolf-Hirschhorn syndrome: Two developmental disorders highlighting the importance of efficient DNA replication for normal development and neurogenesis. DNA Repair (Amst.) *12*, 637–644.
42. Vetro, A., Savasta, S., Russo Raucci, A., Cerqua, C., Sartori, G., Limongelli, I., Forlino, A., Maruelli, S., Perucca, P., Vergani, D., et al. (2017). MCM5: A new actor in the link between DNA replication and Meier-Gorlin syndrome. Eur. J. Hum. Genet. *25*, 646–650.
43. Hughes, C.R., Guasti, L., Meimaridou, E., Chuang, C.-H., Schimenti, J.C., King, P.J., Costigan, C., Clark, A.J.L., and Metherell, L.A. (2012). MCM4 mutation causes adrenal failure, short stature, and natural killer cell deficiency in humans. J. Clin. Invest. *122*, 814–820.
44. Gineau, L., Cognet, C., Kara, N., Lach, F.P., Dunne, J., Veturi, U., Picard, C., Trouillet, C., Eidenschenk, C., Aoufouchi, S., et al. (2012). Partial MCM4 deficiency in patients with growth retardation, adrenal insufficiency, and natural killer cell deficiency. J. Clin. Invest. *122*, 821–832.

45. Cottineau, J., Kottemann, M.C., Lach, F.P., Kang, Y.-H., Vély, F., Deenick, E.K., Lazarov, T., Gineau, L., Wang, Y., Farina, A., et al. (2017). Inherited GINS1 deficiency underlies growth retardation along with neutropenia and NK cell deficiency. J. Clin. Invest. *127*, 1991–2006.
46. Fishel, R., Lescoe, M.K., Rao, M.R., Copeland, N.G., Jenkins, N.A., Garber, J., Kane, M., and Kolodner, R. (1993). The human mutator gene homolog *MSH2* and its association with hereditary nonpolyposis colon cancer. Cell *75*, 1027–1038.
47. Leach, F.S., Nicolaides, N.C., Papadopoulos, N., Liu, B., Jen, J., Parsons, R., Peltomäki, P., Sistonen, P., Aaltonen, L.A., Nyström-Lahti, M., et al. (1993). Mutations of a *mutS* homolog in hereditary nonpolyposis colorectal cancer. Cell *75*, 1215–1225.
48. Rayner, E., van Gool, I.C., Palles, C., Kearsey, S.E., Bosse, T., Tomlinson, I., and Church, D.N. (2016). A panoply of errors: Polymerase proofreading domain mutations in cancer. Nat. Rev. Cancer *16*, 71–81.
49. Palles, C., Cazier, J.-B., Howarth, K.M., Domingo, E., Jones, A.M., Broderick, P., Kemp, Z., Spain, S.L., Guarino, E., Salguero, I., et al.; CORGI Consortium; and WGS500 Consortium (2013). Germline mutations affecting the proofreading domains of POLE and POLD1 predispose to colorectal adenomas and carcinomas. Nat. Genet. *45*, 136–144.
50. Church, D.N., Briggs, S.E.W., Palles, C., Domingo, E., Kearsey, S.J., Grimes, J.M., Gorman, M., Martin, L., Howarth, K.M., Hodgson, S.V., et al.; NSECG Collaborators (2013). DNA polymerase ε and δ exonuclease domain mutations in endometrial cancer. Hum. Mol. Genet. *22*, 2820–2828.
51. Briggs, S., and Tomlinson, I. (2013). Germline and somatic polymerase ε and δ mutations define a new class of hypermutated colorectal and endometrial cancers. J. Pathol. *230*, 148–153.
52. Pachlopnik Schmid, J., Lemoine, R., Nehme, N., Cormier-Daire, V., Revy, P., Debeurme, F., Debré, M., Nitschke, P., Bole-Feysot, C., Legeai-Mallet, L., et al. (2012). Polymerase ε1 mutation in a human syndrome with facial dysmorphism, immunodeficiency, livedo, and short stature ("FILS syndrome"). J. Exp. Med. *209*, 2323–2330.
53. Logan, C.V., Murray, J.E., Parry, D.A., Robertson, A., Bellelli, R., Tarnauskaitė, Ž., Challis, R., Cleal, L., Borel, V., Fluteau, A., et al.; SGP Consortium (2018). DNA polymerase epsilon deficiency causes IMAGe syndrome with variable immunodeficiency. Am. J. Hum. Genet. *103*, 1038–1044.
54. Frugoni, F., Dobbs, K., Felgentreff, K., Aldhekri, H., Al Saud, B.K., Arnaout, R., Ali, A.A., Abhyankar, A., Alroqi, F., Giliani, S., et al. (2016). A novel mutation in the POLE2 gene causing combined immunodeficiency. J. Allergy Clin. Immunol. *137*, 635–638.e1.
55. Weedon, M.N., Ellard, S., Prindle, M.J., Caswell, R., Lango Allen, H., Oram, R., Godbole, K., Yajnik, C.S., Sbraccia, P., Novelli, G., et al. (2013). An in-frame deletion at the polymerase active site of POLD1 causes a multisystem disorder with lipodystrophy. Nat. Genet. *45*, 947–950.
56. Shastry, S., Simha, V., Godbole, K., Sbraccia, P., Melancon, S., Yajnik, C.S., Novelli, G., Kroiss, M., and Garg, A. (2010). A novel syndrome of mandibular hypoplasia, deafness, and progeroid features associated with lipodystrophy, undescended testes, and male hypogonadism. J. Clin. Endocrinol. Metab. *95*, E192–E197.
57. Reinier, F., Zoledziewska, M., Hanna, D., Smith, J.D., Valentini, M., Zara, I., Berutti, R., Sanna, S., Oppo, M., Cusano, R., et al. (2015). Mandibular hypoplasia, deafness, progeroid features and lipodystrophy (MDPL) syndrome in the context of inherited lipodystrophies. Metabolism *64*, 1530–1540.
58. Pelosini, C., Martinelli, S., Ceccarini, G., Magno, S., Barone, I., Basolo, A., Fierabracci, P., Vitti, P., Maffei, M., and Santini, F. (2014). Identification of a novel mutation in the polymerase delta 1 (POLD1) gene in a lipodystrophic patient affected by mandibular hypoplasia, deafness, progeroid features (MDPL) syndrome. Metabolism *63*, 1385–1389.
59. Lessel, D., Hisama, F.M., Szakszon, K., Saha, B., Sanjuanelo, A.B., Salbert, B.A., Steele, P.D., Baldwin, J., Brown, W.T., Piussan, C., et al. (2015). POLD1 germline mutations in patients initially diagnosed with Werner syndrome. Hum. Mutat. *36*, 1070–1079.
60. Nicolas, E., Golemis, E.A., and Arora, S. (2016). POLD1: Central mediator of DNA replication and repair, and implication in cancer and other pathologies. Gene *590*, 128–141.

The American Journal of Human Genetics, Volume *104*

Supplemental Data

Defective DNA Polymerase α-Primase Leads to X-Linked Intellectual Disability Associated with Severe Growth Retardation, Microcephaly, and Hypogonadism

Hilde Van Esch, Rita Colnaghi, Kathleen Freson, Petro Starokadomskyy, Andreas Zankl, Liesbeth Backx, Iga Abramowicz, Emily Outwin, Luis Rohena, Claire Faulkner, Gary M. Leong, Ruth A. Newbury-Ecob, Rachel C. Challis, Katrin Õunap, Jacques Jaeken, Eve Seuntjens, Koen Devriendt, Ezra Burstein, Karen J. Low, and Mark O'Driscoll

Supplemental Note: Case Reports

Clinical descriptions

Family A

The clinical phenotype and linkage analysis in family A has been described before (Van Esch et al. 2005). In summary, the 6 affected males from this 5-generation family showed intellectual disability, growth retardation including microcephaly and hypogonadism. Heights, head circumferences and cognitive levels of carrier females and non-affected males are all within the normal ranges. Carriers females show skewing of X-inactivation (Fig1).

Family B

The index of family B is a 19 years old male born to healthy parents. He has a healthy sister and family history is negative. He has a moderate to severe developmental delay and started to have seizures at the age of 3 months that were difficult to control. His development was from then on severely impaired because of the frequent seizures. He showed pronounced hypotonia, severe feeding problems necessitating feeding via gastrostomy, progressive spasticity, scoliosis, cerebellar hypoplasia and hypogonadotrophic hypogonadism. His healthy mother and sister are carriers of the mutation and show skewing of X-inactivation (Fig 1).

Family C

The index of family C is 5 years old and is the second child of healthy non-consanguineous parents (individual III.2). He has a healthy older brother and younger sister. He was born with an oesophageal atresia with tracheoesophageal fistula repaired day 3 of life. In addition a small interatrial communication with aneurysmal atrial septal tissue was identified in the first year of life. He has moderate developmental delay with speech and language delay being the most pronounced. He has severe microcephaly and short stature fitting in the primordial dwarfism

scale. He has some unusual phenotypic features including deep sacral dimples and a notable lack of subcutaneous fat tissue. His mother, maternal aunt and grandmother are all carriers. His maternal cousin (individual III.5) died at the age of 14 months following a stormy course from birth. He too had severe microcephaly and short stature. After birth he was diagnosed with pulmonary artery stenosis, a VSD and pulmonary atresia. Post operatively he developed a left thalamic bleed, and left subdural effusion. He had a bifid uvula and right vocal cord palsy of unknown aetiology. His medical files documented a hypogonadotrophic hypogonadism. All carriers females show extreme skewing of X-inactivation (Fig 1).

Family D

Individual D is the first child of healthy non-consanguineous parents of Caucasian ancestry. The pregnancy was completed by severe intrauterine growth retardation and maternal eclampsia. Individual D was born at 38 weeks of gestation with a weight of 1.685 kg, length 44.5 cm and HC of 28.5 cm. He continued to grow poorly with the head circumference being particularly affected. At 6 years 11 months, his weight was 14.6 kg (-4.5 SD), height 110.4 cm (-2.6 SD), HC 43 cm (-5.8 SD). Individual D has mild intellectual impairment with impulsive behaviour and a short attention span. He had normal brain MRI Imaging. He has a characteristic facial appearance with up-slanting palpebral fissures and a longish face. He has no other medical problems apart from spina bifida occulta at the L4/L5 level.

Family E

The proband is a 4 year-old male, former dichorionic diamniotic twin conceived via IVF procedure and born at 29 weeks 6 days of gestation. He was diagnosed with intrauterine growth restriction, and currently is below the 3rd centile for height, weight and head circumference. He is developmentally delayed but making progress with specialized speech, occupational, and physical therapy. He has map-like brown pigmentation in the shins but does not display any reticulate hyperpigmentation pattern or hypohidrosis; the skin is abnormally dry

throughout the body. Since birth, the proband has suffered from recurrent infections, including viral illnesses (parainfluenza, recurrent upper respiratory infections), bacterial infections (multiple cases of pneumonia, ear infections, and enterococcus infections), and fungal infections (invasive kidney fungal infection and candidal urinary tract infections). The complete blood count was normal and other than very mild decrease of IgG and IgM levels; there were no other evident changes in the initial evaluation. Lymphocyte proliferation in response to phytohaemagglutinin (PHA) and poke-weed mitogen (PWM) was also normal.

In addition to the *POLA1* variant, the proband and his mother were found to have an *STS* mutation (c.822-1G>A: IVS5-1G>A in intron 5), consistent with X-linked ichthyosis.

Van Esch, H., Zanni, G., Holvoet, M., Borghgraef, M., Chelly, J., Fryns, J.-P., and Devriendt, K. (2005). X-linked mental retardation, short stature, microcephaly and hypogonadism maps to Xp22.1-p21.3 in a Belgian family. European Journal of Medical Genetics 48, 145-152.

Figure S1

Molecular genetic investigations

Family A
(c.236T>G; p.Ile79Ser)

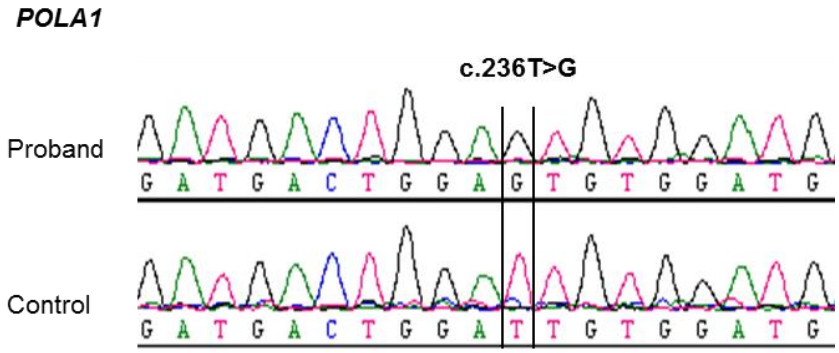

The c.236T>G mutation in the DNA sample of the index case (top) compared to a healthy, unrelated control.

Family B
(c.4142C>T; p.Pro1381Leu)

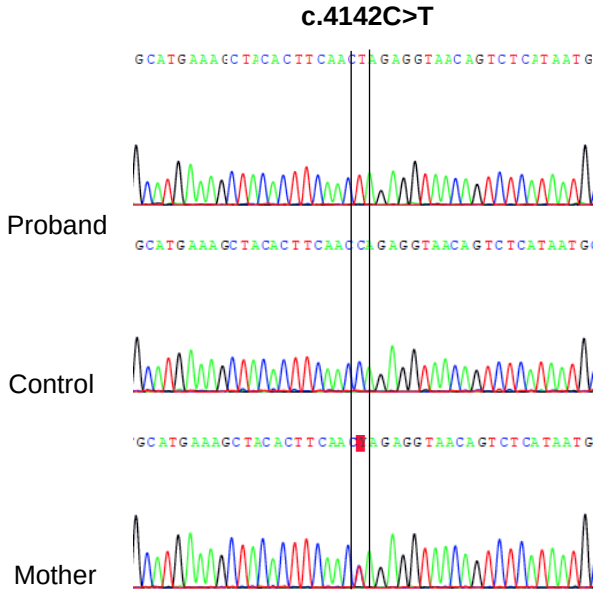

The c.4142C>T mutation in the DNA sample of the index case (top) compared to a healthy, unrelated control. The mother is a carrier of the mutation.

Family C

(c.507+1G>A; p.(Lys149_Glu169del,Thr170_Ser1462delins15*)

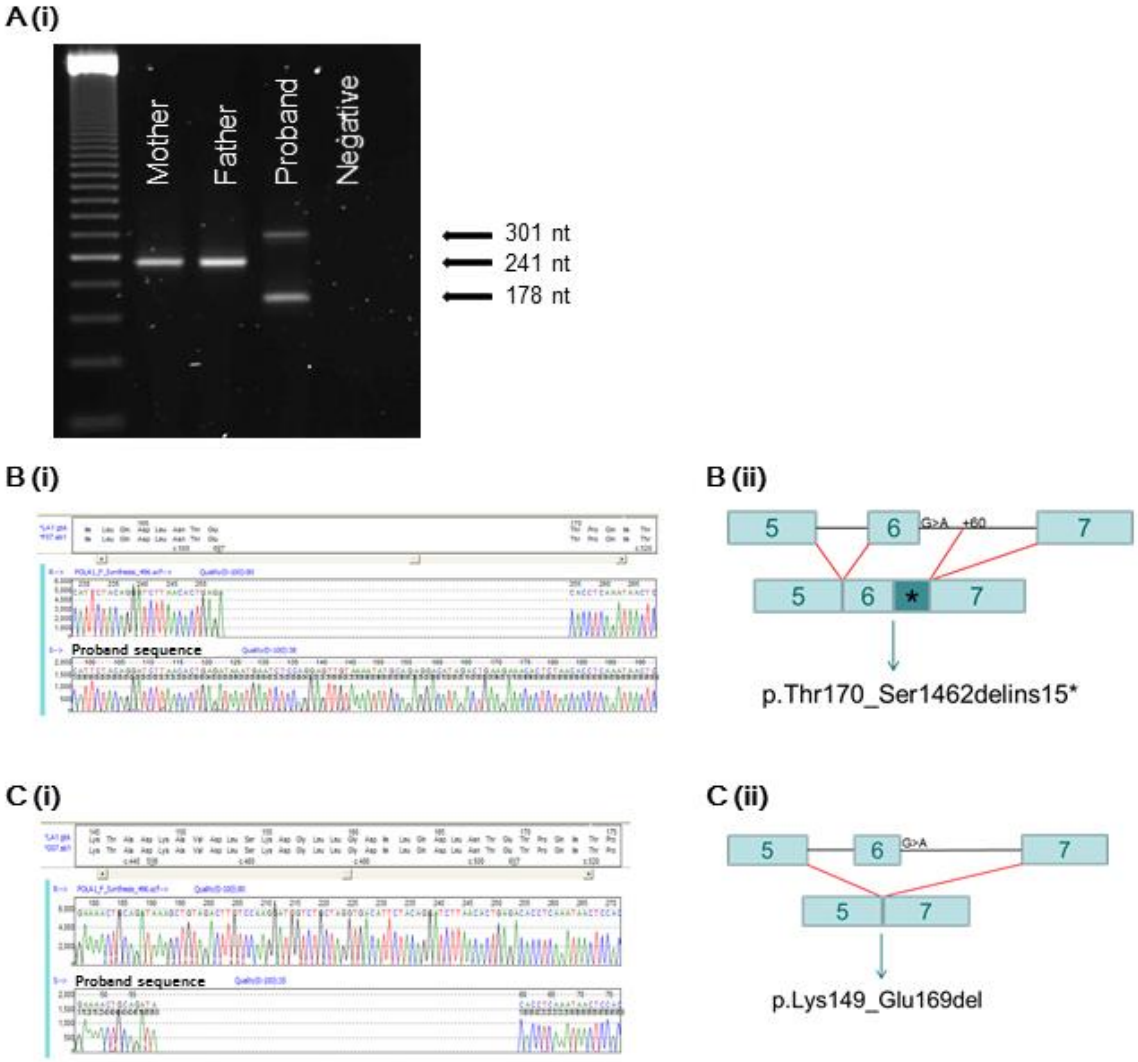

The c.507+1G>A splice-site variant was predicted to completely abolish the donor splice site using 5 different splicing prediction programs (MaxEnt: -100.0%, NNSPLICE: -100.0%, Human Splicing Finder: -100.0%, SpiceSite Finder-like: -100.0%, GeneSplicer -100.0%, accessed through Alamut Visual v.2.7.1 software).

A. cDNA analysis of *POLA1* RNA transcripts from peripheral blood in mother, father and proband. Parents show a normally spliced RNA transcript containing exons 5, 6 and 7 (241nt).

The proband did not express the normal transcript, but expressed two abnormal transcripts of 301nt and 178nt.

B. (i) Sanger sequencing of the 301nt band revealed that this transcript contains an insertion of the first 60 nucleotides of intron 6, r.507_508ins507+1_507+60. (ii) Activation of a cryptic splice donor site within intron 6 is predicted to result in the insertion of 15 amino acids and the introduction of a premature termination codon p.(Thr170_Ser1462delins15*).

C. (i) Sanger sequencing of the 178nt band revealed that this transcript contains a deletion of exon 6, r.445_507del. (ii) This is an in-frame deletion, predicted to produce a protein product lacking the 21 amino acids encoded by exon 6, i.e. p.(Lys149_Glu169del).

Family D

(c.445_507del; p.Lys149_Glu169del)

A

B

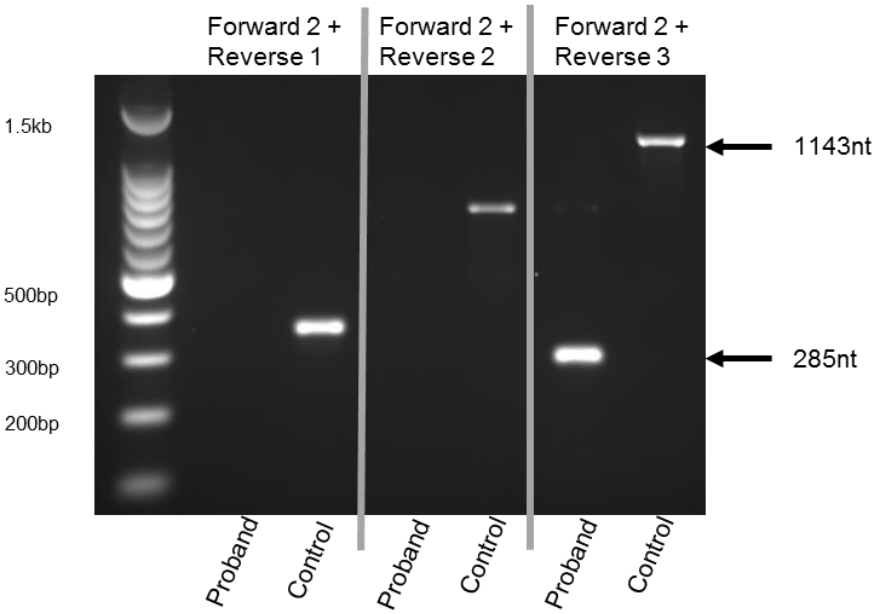

C

Analysis of exome data in the index of family D indicated a hemizygous deletion involving exon 6 of *POLA1*. This was confirmed by PCR, using different combinations of primers as shown in panels **A** and **B**. Only with primers Forward2 and Reverse3 a PCR product was obtained in the index, and subsequent sequencing of this product confirmed the deletion (the blue underlined sequence is present in the PCR product of 285 nt).

C. The deletion of exon 6 leads to an in-frame deletion of 21 amino acids.

Family E

(c.328G>A; p.Gly110Arg)

A

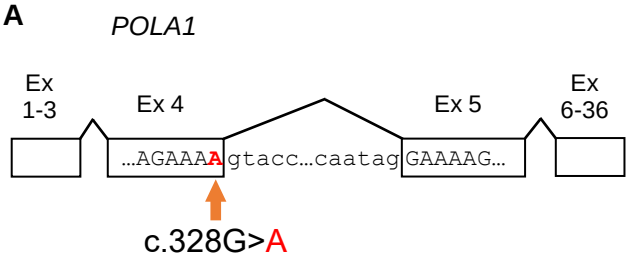

B

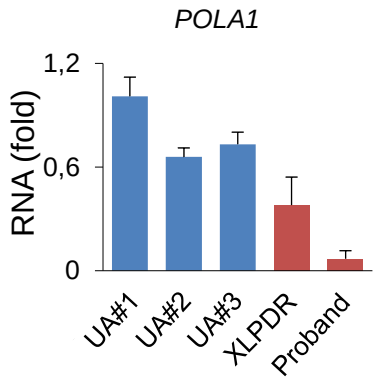

A. Schematic representation of *POLA1* and the location of the mutation (red arrow).

B. *POLA1* mRNA expression by qRT-PCR in dermal fibroblasts derived from 3 unaffected (UA) males, an XLPDR individual, and the proband described here. Data are representative of more than 5 replicates, bars – S.E.M. The experimental details are described in Materials and Methods section.

Figure S2

Conservation of missense variants and pathogenicity scores

Ile 79. **Family A: Ile79Ser**

Human	47	YK----YEV-EDFTGVYEEVDEEQYSKLVQARQDD--DWIVDDD---GIG	86
Chimpanzee	47	YK----YEV-EDFTGVYEEVDEEQYSKLVQARQDD--DWIVDDD---GIG	86
Rhesus macaque	47	YK----YEV-EDFTGVYEEVDEEQYSKLVQARQDD--DWIVDDD---GIG	86
Dog	53	YK----YEV-EDFTSVYEEVDEEQYSKLVQARQDD--DWIVDDD---GIG	92
Cow	47	YK----YEV-EDFTSVYEEVDEEQYSKLVQARQDD--DWIVDDD---GIG	86
Mouse	53	YK----YEV-EDLTSVYEEVDEEQYSKLVQARQDD--DWIVDDD---GIG	92
Rat	53	YK----YEV-EDLTSVYEEVDEEQYSKLVQARQDD--DWIVDDD---GIG	92
Chicken	94	LK----YEV-EEFTGVYDEIDEEQYSKIVRERQDD--DWIVDDD---GIG	133
Zebrafish	55	VK----YEV-EEFTSIYDEVDEEQYSKIVRERQDD--DWIIDDD---GTG	94
Frog	38	VK----YEV-EEISSIYEEVDEEQYSKIVRDRQDD--DWIVDDD---GTG	77

Gly 110. **Family E: Gly110Arg**

Human	87	YVEDGREIF--DDD--LEDDALDADEKG---------KDGKARNKDKRNV	123
Chimpanzee	87	YVEDGREIF--DDD--LEDDALDADEKG---------KDGKARNKDKRNV	123
Rhesus macaque	87	YVEDGREIF--DDD--LEDDALDAGEKG---------KDGKARNKDKRNV	123
Dog	93	YVEDGREIF--DDD--LEDDALDSHEKG---------KDDKARTKDRRNV	129
Cow	87	YVEDGREIF--DDD--LEDDALDSHEKG---------KDNKACNKDKRTV	123
Mouse	93	YVEDGREIF--DDD--LEDDALDTCGKG---------SDGKAHRKDRKDV	129
Rat	93	YVEDGREIF--DDD--LEDDALDTCGEG---------SDGKAHRKDRKDV	129
Chicken	134	YVEDGREIF--DED--LDDDALGSSKKG---------KTGKTSTIGKKNV	170
Zebrafish	95	YVEDGREIF--DEE--LDDDALG-PKTG---------KQAAKGGDSKKNV	130
Frog	78	YVEDGREIF--DDD--LEDNAL--ADSG---------KRAKGAPKDKSNV	112

Pro 1381. **Family B: Pro1381Leu**

Human	1362	LQF---SRTGPLCP--------ACMK--ATLQPEYSDKSLYTQLCFYRYI	1398
Chimpanzee	1281	LQF---SRTGPLCP--------ACMK--ATLQPEYSDKSLYTQLCFYRYI	1317
Rhesus macaque	1362	LQF---SRTGPLCP--------ACMK--ATLRPEYSDKSLYTQLCFYRYI	1398
Dog	1368	LQF---SRNGPLCQ--------VCMK--ATLRPEYSDKSLYTQLCFYRYI	1404
Cow	1362	LQF---SRNGPLCQ--------VCMK--ATLRLEYSDKSLYTQLCFYRYI	1398
Mouse	1366	LHF---SRNGPLCP--------VCMK--AVLRPEYSDKSLYTQLCFYRYI	1402
Rat	1369	LHF---SRNGPLCP--------ACMK--AVLRPEYSDKSLYTQLCFYRYI	1405
Chicken	1438	LSF---SRSGPICQ--------ACRK--AILRPEYSDKALYTQLCFYRYI	1474
Zebrafish	1370	IAF---SRSGPICP--------ACLR--STLKPEYSEKALYNQLSFYRYI	1406
Frog	1366	LSF---SRNGPICQ--------ACTK--ATLRSEYPEKALYTQLCFYRFI	1402

Conservation of the *POLA1* missense variants. Alignments were generated using MUSCLE (version 3.6 using maxiters 2), comparing the amino acid sequences within and around the sites of the three human missense mutants identified in this study (highlighted in yellow), to that of other vertebrates. The high degree of conservation of Ile79 and Gly110 is evident. Pro 1381 is also highly conserved. It's worth noting that as aa1381 is Leu in the cow POLα, sequence identity across the entire cow POLα compared to human is 90.6%. This is lower than that of chimpanzee (98.2%) and rhesus macaque (97.7%). Specific accession numbers are as follows; Human: NP_058633.2, Chimpanzee: XP_003317445.2, Rhesus macaque: XP_001091195.1 Dog: XP_005641271.1, Cow: NP_001192994.1, Mouse: NP_032918.1,

Rat: NP_445931.1, Chicken: XP_416792.3, Zebrafish: XP_005162809.1, Frog: XP_004911812.1.

Software	Variant & Score		Classification comment
PolyPhen2	**I79S:**	1	Probably damaging
	G110R:	0.247	Benign
	P1381L:	0.001	Benign
PROVEAN	**I79S:**	-4.190	Deleterious
	G110R:	-1.365	Neutral
	P1381L:	-2.919	Deleterious
MutationTaster	**I79S:**	142	Disease causing
	G110R:	125	Disease causing
	P1381L:	98	Disease causing
Align GVGD	**I79S:**	Class C65	Most likely to interfere with function
	G110R:	Class C65	Most likely to interfere with function
	P1381L:	Class C65	Most likely to interfere with function

Pathogenicity predictions. A summary of the pathogenicity predictions for each missense mutation generated using the following pathogenicity prediction software tools:

PolyPhen2 (http://genetics.bwh.harvard.edu/pph2/),

PROVEAN (http://provean.jcvi.org/index.php),

MutationTaster (http://mutationtaster.org/)

Align GVGD (http://agvgd.hci.utah.edu/).

Figure S3

Chromatin localisation of POLα-primase subunits p180-POLα, p68-POLA2 and p48-PRIM1.

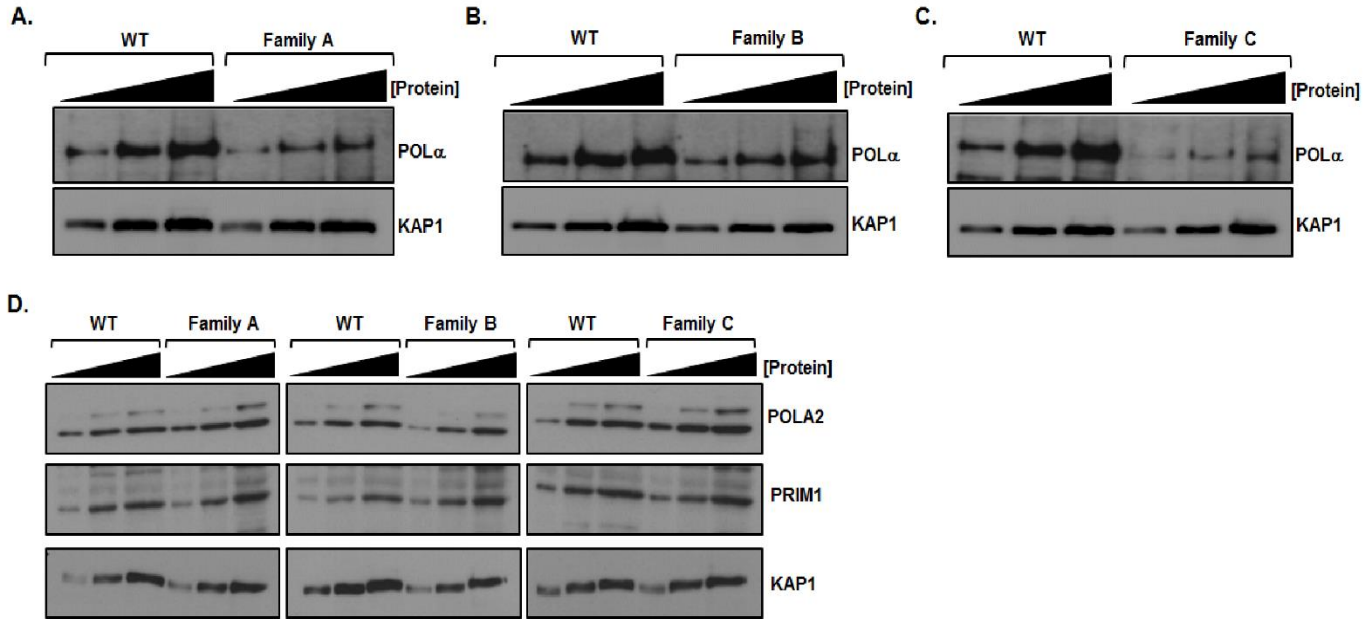

A. Increasing amounts of chromatin extracts from wild-type (WT) and family A patient LCLs were assessed for POLα levels. A very modest reduction in POLα chromatin retention was seen in extracts from Family A, although this not a significant reduction.

B. Chromatin extracts from family B LCLs exhibited a similar finding to that of family A.

C. Consistent with WCE analysis, *POLA1*-mutant LCLs from family C also exhibited a marked reduction of POLα on chromatin.

D. Western analysis of chromatin extracts for the POLα-primase subunits p68-POLA2 and p48-PRIM1 from each of the proband LCLs from families A, B and C did not reveal any marked differences in subunit chromatin retention. This suggests that the stoichiometry of POLα-primase components enriched on chromatin is preserved.

Figure S4

LCL proliferation analysis.

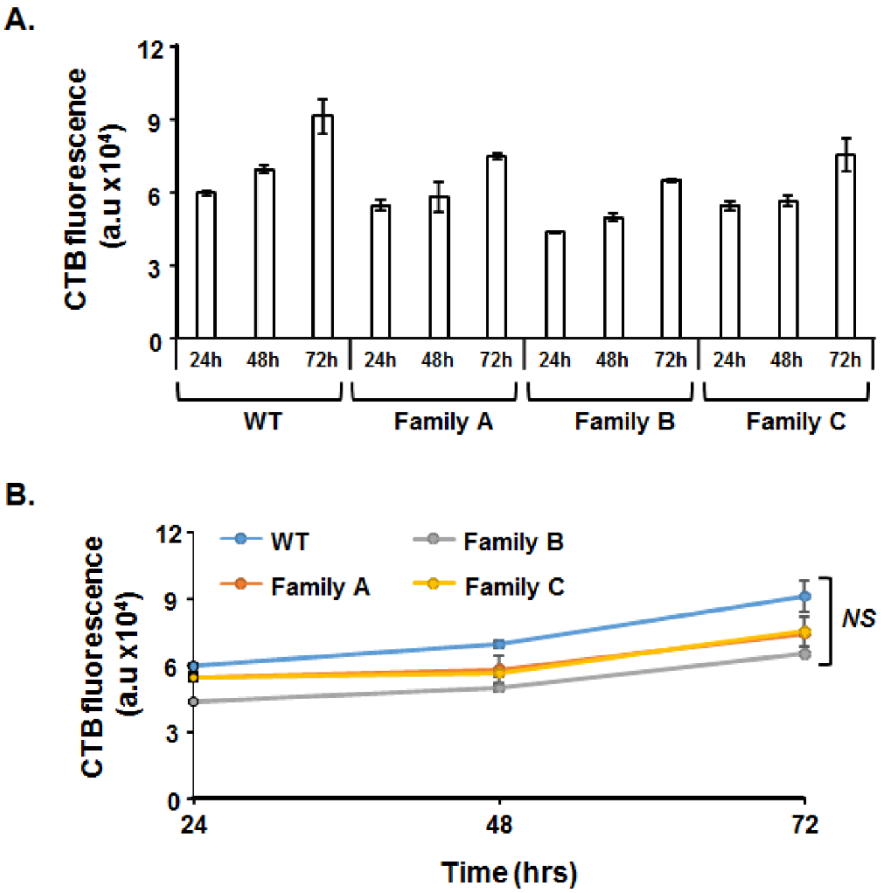

A. 1x10^4 cells were seeded in 100µl in triplicate into a 96 well plate and proliferation was assessed over 24hrs-72hrs using CellTitre-Blue fluorescence proliferation assay. The fluorescence output from each LCL at 24h, 48h and 72h is shown as a bar chart. From Fig 4C; % EdU positive cells (30 min pulse) from untreated (Unt) LCLs from the father (25.86 ± 3.57) and mother (34.78 ± 5.17) compare highly to that of the family C proband (24.44 ± 4.28%). From Fig 4D a similar outcome is evident; % EdU positive cells from untreated (Unt) LCLs from WT (26.84 ± 4.92%) are highly similar to those of both affected individuals from Family A (V-4: 23.31 ± 3.03% and IV-7: 21.31 ± 1.59%) and the proband of family B (22.06 ± 2.72%).

B. This is a line graph depiction of the same fluorescence shown in A, indicating the similar slope between the wild-type (WT) LCLs and those of the probands from families A, B and C. (WT: *m*>652.4, Family A: *m*>413.2, Family B: *m*>444.3, Family C: *m*>432). *NS*; not statistically significant at 72hrs *p=0.376 (Student's t test).*

Figure S5

DNA replication following *POLA1* siRNA

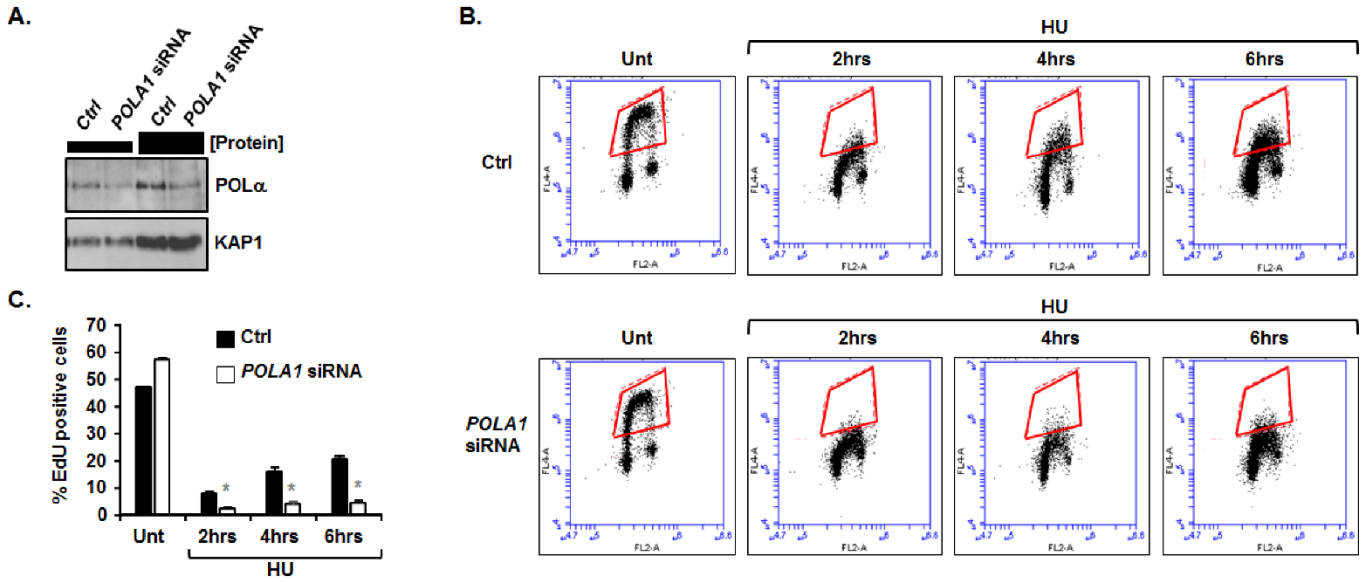

A. U2OS cells were subjected to *POLA1* siRNA (24hrs) with the intention of obtaining a partial and not complete reduction in POLα expression levels. Under these conditions, a reduction of ~60% in POLα levels from whole cell extracts was observed following *POLA1* siRNA compared to control (Ctrl) scrambled siRNA.

B. The impact of mildly stressing conditions (125μM HU) upon DNA replication was assessed via EdU-pulse incorporation (30mins) in untreated (Unt) cells, and at the times indicated post treatment with HU, using flow cytometry of U20S following control (Ctrl) scramble siRNA and *POLA1* siRNA. Representative flow cytometry panels are shown; the red hatched area denotes EdU positive cells. The panels show a marked reduction in EdU incorporation in the *POLA1* siRNA cells at all-time points following HU, compared to the control (Ctrl) conditions.

C. The bar chart shows EdU incorporation in untreated (Unt) and HU treated U2OS following control (Crtl) and *POLA1* siRNA, indicating the significant reduction in DNA replication under these conditions in U2OS cells under-expressing POLα (*POLA1*) *(**asterisks** indicate p<0.05 Student's t test).*

Materials and methods

Cell culture

EBV-transformed lymphoblastoid cell lines (LCLs) derived from affected individuals, indicated parents or an unrelated wild-type (WT) phenotypically normal individual were cultured in RPMI1640 with 15% foetal calf serum (FCS), antibiotics (Pen-Strep) and L-Gln. Cells were maintained at 37ºC in humidified incubators under 5% CO_2. LCL proliferation was assessed using CellTitre-Blue reagent kit (G8080) according to manufacturers' instructions (Promega). U2OS cells were similarly maintained but cultured in DMEM supplemented with 10% FCS, Pen-Strep and L-Gln.

Antibodies

DNA Polα (G16) goat polyclonal (sc-5921), POLA2 (D2) mouse monoclonal (sc-398255) and PRIM1 (H9) mouse monoclonal (sc-390265) were obtained from Santa Cruz Technologies Ltd and used for blotting extracts from the LCLs. For the dermal fibroblasts we used anti- POLA1 from ThermoFisher (PA5-36147) and anti-β-Actin from Sigma-Aldrich (A5441). The antibodies used for DNA fibre combing included mouse anti-BrdU (Becton Dickinson 347580) for IdU detection, rat anti-BrdU (Abcam Ab 6326) for CldU detection, rat anti-single strand DNA (Genomic Vision). Secondary antibodies were Alexa Fluor (Invitrogen) anti-rat 488 (A21208), anti-mouse 594 (A31624) and anti-rabbit 647 (A31573).

Cell extracts

LCLs were washed in PBS then lysed in Urea-based lysis buffer (9M urea, 50mM Tris-HCl at pH 7.5, 10mM β-mercaptoethanol), followed by a sonication at 30% amplitude (12 sec). Protein concentration was determined by Bradford Assay. For chromatin extract preparation cells were washed in ice-cold PBS, resuspended in hypotonic buffer (10 mM HEPES pH 7.5, 5mM KCl, 1.5 mM $MgCl_2$, 1mM DDT, 10 mM NaF, 1 mM Na_2VO_3, 10 mM β-glycerophosphate, 0.5% IGEPAL and Roche protease inhibitor cocktail) and incubated on ice for 15 min. The sample was pelleted and washed twice in hypotonic buffer and resuspended in hypotonic buffer containing 0.5 M NaCl and incubated for 15 min on ice. Resultant chromatin was then

pelleted (17,000*xg* for 10 min) and solubilised in urea-based lysis buffer. For the dermal fibroblasts, whole cell lyates were prepared using Triton lysis buffer (25mM HEPES, 100mM NaCl, 10mM DTT, 1mM EDTA, 10% glycerol, 1% Triton X-100) supplemented with 1mM sodium orthovanadate and protease inhibitors (Roche).

Fibre combing and microscopy

DNA fibres were combed from genomic DNA agarose plugs using the FiberComb Molecular Combing System (Genomic Vision) and processed for immunofluorescence according to the manufacturer's instructions. Images were captured and processed using the Olympus IX70 Fluorescence microscopy platform. A conversion factor of 2kb/μm was used as is standard for combed fibres and fibre track lengths processed using BoxPlotR.

Flow cytometry

LCLs were treated with 125μM HU for the indicated times and pulse labelled with EdU (10μM) 30mins prior to the end of each time point, then processed using Click-iT EdU Alexa Fluor-647 imaging kit according to the manufacturer's instructions (ThermoFisher Scientific). Samples were counterstained with propidium iodide (5μg/ml), analysed using BD Accuri C6 Plus flow cytometer and profiles processed using BD CSampler software.

siRNA

U2OS were transfected with *POLA1* siRNA oligonucleotides using Lipofectamine RNAmax (Invitrogen) and assessed 24hrs post-transfection. A combination of two 3'-UTR directed POLA1 oligonucleotides was used; sense, 5'-UCGUAAGCAUCAUAGAAAUUU-3' and sense, 5'-CAAUUAAACCCGGUCUAAAUU-3'.

In situ hybridisation

Digoxigenin (DIG) labelled sense and antisense PCR probes (DIG RNA labelling kit, Roche) were designed using the F primer with a SP6 promotor site: 5'-CATTTAGGTGACACTATAGAAAGGGAGTTTTGCAGCTTCC-3' and a R primer with a T7 promotor site: 5'- TAATACGACTCACTATAGGGAGGTGGTGGAGTTATTTGAGC-3'. By

means of sequencing we verified the PCR product obtained for *Pola1*. The labelled RNA sample was purified by ethanol precipitation and the sample was size separated on a 2% agarose gel. Timed pregnant (E0.5 is the morning of the day of vaginal plug) Swiss females were dissected and brains of E16.5 mouse embryos were collected and washed in ice-cold PBS. Postnatal brains were isolated after perfusion with PBS and 4% paraformaldehyde. All material was fixed overnight with 4% paraformaldehyde followed by progressive alcohol-assisted dehydration and paraffin embedding. Frontal 6 µm thick sections were processed for *in situ* hybridization using an automated platform (Ventana Discovery, Ventana Medical Systems; details of procedures can be obtained at request), dehydrated and mounted with Eukitt (Sigma). Photographs were taken on a Leica DM5500B microscope.

qRT-PCR Family E

RNA was extracted using Trizol (Invitrogen) according to the manufacturer's instructions. Total RNA (5µg) was used for cDNA synthesis utilizing the Superscript III strand synthesis system (Invitrogen). Quantitative real-time RT-PCR was performed using a Mastercycler (Eppendorf, Germany) following manufacturer's recommendations. SYBR Green based detection (Invitrogen) was employed using the following gene specific primers:

Target	**Forward**	**Reverse**
ACTB	GCGGGAAATCGTGCGTGACATT	GATGGAGTTGAAGGTAGTTTCGTG
POLA1 full	GCTATGTGGAAGATGGCCGA	TGTTCGGTTTTGTCACTGCG

Experiments were performed in duplicate, data were normalized to housekeeping genes, and the relative abundance of transcripts was calculated by the comparative *ΔΔCt* method.

X-chromosome inactivation

Lymphocyte-derived genomic DNA was subjected to the androgen-receptor gene methylation assay for assessment of the methylation status [Allen et al., 1992]. A ROX-labeled genotyping marker 100-500 (Applied Biosystems) was added and the samples were

separated on an ABI3130xl automated DNA sequencer (Applied Biosystems) and analyzed with the GeneMapper analysis software (Applied Biosystems) for peak position and area intensity calculations.

Allen, RC., Zoghbi, HY., Moseley, AB., Rosenblatt, HM., Belmont, JW. (1992). Methylation of HpaII and HhaI sites near the polymorphic CAG repeat in the human androgen-receptor gene correlates with X chromosome inactivation. Am. J. Hum. Genet. 51(6), 1229-39.